Mon. Not. R. Astron. Soc. **000**, ??–?? () Printed 6 April 2009 (MN LATEX style file v2.2)

Redistributing hot gas around galaxies: do cool clouds signal a solution to the overcooling problem?

Tobias Kaufmann[1] ⋆, James S. Bullock[1], Ariyeh H. Maller[2], Taotao Fang[1] and James Wadsley[3]
[1] *Center for Cosmology, Department of Physics and Astronomy, University of California, Irvine, CA 92697*
[2] *Dept. of Physics, New York City College of Technology, CUNY, NY, 11201*
[3] *Department of Physics & Astronomy, McMaster University, 1280 Main St. West, Hamilton ON L8S 4M1 Canada*

6 April 2009

ABSTRACT
We present a pair of high-resolution smoothed particle hydrodynamics (SPH) simulations that explore the evolution and cooling behavior of hot gas around Milky-Way size galaxies. The simulations contain the same total baryonic mass and are identical other than their initial gas density distributions. The first is initialised with a *low entropy* hot gas halo that traces the cuspy profile of the dark matter, and the second is initialised with a *high-entropy* hot halo with a cored density profile as might be expected in models with pre-heating feedback. Galaxy formation proceeds in dramatically different fashion depending on the initial setup. While the low-entropy halo cools rapidly, primarily from the central region, the high-entropy halo is quasi-stable for $\sim$ 4 Gyr and eventually cools via the fragmentation and infall of clouds from $\sim$ 100 kpc distances. The low-entropy halo's X-ray surface brightness is $\sim$ 100 times brighter than current limits and the resultant disc galaxy contains more than half of the system's baryons. The high-entropy halo has an X-ray brightness that is in line with observations, an extended distribution of pressure-confined clouds reminiscent of observed populations, and a final disc galaxy that has half the mass and $\sim$ 50% more specific angular momentum than the disc formed in the low-entropy simulation. The final high-entropy system retains the majority of its baryons in a low-density hot halo. The hot halo harbours a trace population of cool, mostly ionised, pressure-confined clouds that contain $\sim$ 10% of the halo's baryons after 10 Gyr of cooling. The covering fraction for H I and Mg II absorption clouds in the high-entropy halo is $\sim$ 0.4 and $\sim$ 0.6, respectively, although most of the mass that fuels disc growth is ionised, and hence would be under counted in H I surveys.

Key words: galaxies: formation — hydrodynamics — methods: numerical — methods: N-body simulations.

1 INTRODUCTION

It is well known that in the absence of feedback the majority of baryons in galaxy-size dark matter haloes ($M \sim 10^{12}$ M$_\odot$) should have cooled into halo centres over a Hubble time (e.g. White & Rees 1978; Katz 1992; Benson et al. 2003). In contrast, only $\sim$ 20% of the associated baryons in Milky-Way size haloes are observed to be in a cold, collapsed form (Maller & Bullock 2004 (MB04); Mo et al. 2005; Fukugita & Peebles 2006; Nicastro et al. 2008). An understanding of the feedback processes that act to solve this galaxy overcooling problem is a major goal of galaxy formation today. It is not known if the undiscovered galactic baryons exist primarily in hot gaseous halos around normal galaxies (MB04; Fukugita & Peebles 2006; Sommer-Larsen 2006) or if they have been mostly expelled as a result of energetic blow-out (e.g., Dekel & Silk 1986; Oppenheimer & Davé 2006).

There are several reasons to take seriously the possibility that a large fraction of the missing galactic baryons reside in the halos of normal galaxies. In the Milky Way, X-ray absorption lines produced by local hot gas are detected in the spectra of several bright AGN (e.g., Williams et al., 2005; Fang et al., 2006). Many argue that this absorption corresponds to local gas ($\sim$ 50 kpc; e.g., Wang et al., 2005; Fang et al., 2006; Bregman & Lloyd-Davies, 2007), but the true origin of these features, including whether it

⋆ E-mail: tobias.kaufmann@uci.edu

is associated with a hot component of the Milky Way disc or with an extended hot halo, remains open to debate. Interestingly, Sembach et al. (2003) and Tripp et al. (2003) have argued that high-velocity features observed by FUSE highlight the boundaries between HI clouds (High-Velocity Clouds, HVCs) and an extended, hot gaseous corona around the Galaxy. Further indirect evidence for a hot Galactic halo comes from ram-pressure stripping models the Magellanic stream (e.g., Mastropietro et al. (2005); Kaufmann et al. in preparation) and the lack of neutral gas in low-luminosity satellite galaxies of the Milky Way (Grcevich et al., 2008). The HVCs themselves might be the neutral cores of larger, pressure-supported clouds embedded within this hot gas halo (MB04; Collins et al. 2005; Thom et al. 2006; Peek et al. 2007).

Quasar absorption line studies suggest that normal Milky-Way-type galaxies at intermediate redshift are surrounded by extended, $\sim$ 100 kpc, haloes of cool gas clouds ($T \simeq 10^4 - 10^5$ K) with high covering factors ($f \sim 0.6-0.8$). Less massive galaxies tend to have smaller, less pronounced gaseous haloes (Steidel, 1995; Chen et al., 2001; Tumlinson & Fang, 2005; Kacprzak et al., 2008; Chen & Tinker, 2008) and the probability that cool halo gas is present may correlate with the color of the galaxy (Barton & Cooke in preparation). Interestingly, however, X-ray observations place tight constraints on the nature of hot gas around nearby disc galaxies. Specifically, it must be of a relatively low density in order to evade X-ray emission bounds (recent limits include $S_x < 10^{-14}$ erg cm^{-2} s^{-1} arcmin^{-2}, Pedersen et al. 2006; $L_X < 3.8 \times 10^{41}$ erg s^{-1}, Benson et al. 2000; $L_X < 3 \times 10^{39}$ erg s^{-1}, Li et al. 2007). These results, together with the fairly high covering factors in cool clouds implied by absorption line studies may suggest a picture where normal galaxies are surrounded by extended, low-density hot ($\sim 10^6$ K) haloes that are filled with fragmented, pressure supported cool ($\sim 10^4$ K) clouds (MB04; Mo & Miralda-Escude 1996).

Independently, models aimed at explaining the optical properties of galaxies have relied increasingly on the idea that extended, quasi-stable hot gas haloes develop around massive galaxies (Birnboim & Dekel 2003; Kereš et al. 2005; Bower et al. 2006, Croton et al. 2006; Dekel & Birnboim 2006). It is suggested that these hot haloes may be quite susceptible to feedback mechanisms, which could stabilise the systems to cooling and help explain the observed bimodality in galaxy properties (Dekel & Birnboim 2006). It is possible that in massive galactic haloes (a few times 10^{12} M$_\odot$) gravitational quenching by clumpy (fragmentary) accretion could provide the source of energy (Dekel & Birnboim 2008).

Observational probes of the gaseous haloes of galaxies provide a potential means of testing these ideas. Entropy injected from feedback mechanisms will alter the density distribution of halo gas and affect associated cooling rates (and thus X-ray emission) and the distribution of cooling clouds fragmenting within the hot haloes. Similarly, early feedback or *pre-heating* before the halo collapses can affect halo gas profiles in a related manner, with positive consequences for galaxy properties at $z = 0$ (Mo & Mao 2002; Oh & Benson 2003; Lu & Mo 2007). This type of feedback has the potential for solving many of the major problems in galaxy formation. Not only will it help with overcooling, but it may also result in larger disc galaxies, relieving the so-called angular-momentum problem (Navarro & Steinmetz 2000, Maller & Dekel 2002). Moreover, the X-ray emission in pre-heated haloes is expected to stay within observational bounds (Mo & Mao 2002). The degree to which this type of pre-heating may affect the fraction of material accreted directly in the form cold flows that do not shock-heat (Birnboim & Dekel 2003; Kereš et al. 2005) has yet to be investigated.

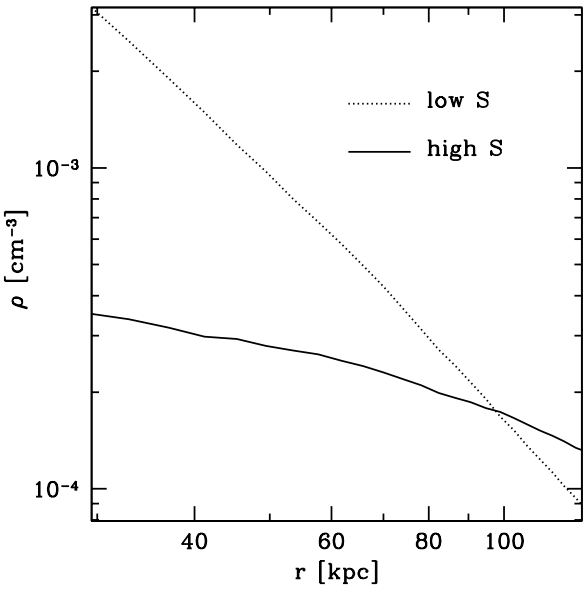

Figure 1. Initial gas density profiles for our low and high entropy models. Note that both models have the same total gas mass within their virial radii. The profiles shown have been evolved with an adiabatic equation of state in order to achieve full relaxation.

In this paper we begin to address some of these questions by simulating the formation of a Milky Way sized spiral galaxies starting with two different initial conditions. We focus specifically on the cooling of hot halo baryons – a process that is expected to be important in fueling galaxy assembly at $z < 1$ in dark matter haloes of mass $\sim 10^{12} M_\odot$ (after the epoch of cold-mode accretion has ended for these objects, Kereš et al. 2009; Brooks et al. 2009). Note that $10^{12} M_\odot$ dark matter haloes grow rapidly at high redshift, but then grow slowly after $z \sim 1$ (Wechsler et al. 2002; Zhao et al. 2008) and usually do not experience major ($> 1/3$) mergers since that time (Maller et at. 2006, Stewart et al. 2008). Therefore while our simulations do not model the early growth of the galaxy well, they likely provide a reasonable estimate of late-time cooling flow behaviour.

The first case we consider has a hot gas profile that traces the density profile of the dark matter. This, our *low-entropy* halo case, has the lowest central entropy in hot gas that could realistically be expected. Our second case explores cooling from a *high-entropy* hot halo, which has a significant core in its density profile at small radius. This hot halo has a central entropy value of $S \sim 30$ keV cm^2, which is well within range expected (and seen) in cosmological simulations that include substantial non-gravitational pre-heating sources (e.g. Davé et al. 2008 find central entropy values of $S \sim 100$ keV cm^2 in small group haloes of mass $\sim 10^{12.7} M_\odot$ as a result of feedback from outflows).

Table 1. Simulated galaxies. The fiducial models are shown in the upper part, the runs investigating resolution and temperature dependence are shown in the lower parts.

(1) Name	(2) # gas particles	(3) T_F [10^4 K]	(4) Softening Length [kpc]	(5) Gas Particle Mass [$M_\odot$]	(6) Dark Matter Particle Mass [$M_\odot$]	(7) $E_{tot}(t=0)$ [erg]
low entropy	5×10^5	3.0	0.514	2.8×10^5	2.5×10^6	-3.09×10^{59}
high entropy	5×10^5	3.0	0.514	3.6×10^5	2.5×10^6	-2.91×10^{59}
low entropy low-resolution	1×10^5	3.0	0.514	1.4×10^6	1.3×10^7	
high entropy low-resolution	1×10^5	3.0	0.514	1.8×10^6	1.3×10^7	
high entropy high-resolution	2×10^6	3.0	0.257	9.0×10^4	6.3×10^5	
high entropy LT	5×10^5	1.5	0.514	3.6×10^5	2.5×10^6	

(3) T_F is the imposed temperature floor, LT in the name indicates a low temperature floor.
(7) The total energy content of the halo after the evolution with the adiabatic EOS.

Another possibility is that dynamical processes could be responsible for creating hot gas halo profiles of this kind (Kereš et al. 2009; Dekel & Birnboim 2008; Conroy & Ostriker 2008; Khochfar & Ostriker 2008). We evolve these two haloes in isolation without any (additional) form of feedback for 10 Gyr to explore three questions. One, can large, low-density, hot haloes of the kind suggested by observations exist in a quasi-stable state for cosmological time-scales? Two, can changes to circum-galactic hot gas at high redshifts persist until today? And three, do different initial conditions and cooling histories create features that are observable in galaxies and their gaseous halos today?

In Section 2, we present our initial conditions and the numerical techniques. In Section 3, we discuss the resulting gas halo properties after 10 Gyr of cooling and discuss these results in the context of gas halo observations. The time evolution of the hot haloes as they cool and form central galactic discs are studied in section 4. Section 5 presents a discussion of numerical convergence. We conclude and summarise in Section 6.

2 SMOOTHED PARTICLE HYDRODYNAMIC SIMULATIONS

We simulate isolated systems with virial mass similar to the Milky Way. Haloes are initialised as spherical equilibrium profiles using the methods outlined in Kazantzidis et al. (2004). The virial mass of the model is $M_{200} = 10^{12} M_\odot$ and the dark haloes have NFW density profiles (Navarro, Frenk & White 1996) characterised by a halo concentration $c = 8$, where the concentration is defined as $c = \frac{R_{200}}{R_s}$, where R_s is the halo scale radius and $R_{200} = 206$ kpc is the virial radius of the halo (radius corresponding to a density of 200 times the critical density). Table 1 lists the specific parameters used in each simulation and provides a reference name for each run.

2.1 Initial conditions

We initialise a fraction of the total halo mass, $f_\mathrm{b} = 0.1$, as a hot baryonic component with either the same radial distribution of density as the dark matter (the *low-entropy* model) or with a flat entropy profile that results in a a shallower density profile (the *high-entropy* model), as shown in Figure 1. Note, that all the models start with the same amount of baryons within the virial radius of the halo. We then impose a temperature profile such that the gas is initially in hydrostatic equilibrium for an adiabatic equation of state (EOS) where gas cooling is turned off. The high entropy model has a central entropy parameter, $S_0 = T_0/n_0^{2/3} \simeq 30$ keV cm^2 of the type suggested in scenarios with substantial pre-heating (e.g. Mo & Mao 2002). The amount of entropy in the low entropy model is likely lower than values arising in cosmological simulations, therefore providing a lower limit in terms of entropy content. However, the assumption that the hot gas follows the radial distribution of the dark matter is widespread in the literature (e.g. van den Bosch 2001). For all of our fiducial models we choose $\lambda_g = 0.03$ for our gas spin parameter, defined in analogy with the halo spin as $\lambda_g \equiv j_g |E|^{1/2} G^{-1} M_{200}^{-3/2}$. Here, j_g is the average specific angular momentum of the gas, E and M_{200} are the total energy and mass of the *halo*.

The specific angular momentum distribution of the gas is assumed to scale linearly with the cylindrical distance from the angular-momentum axis of the halo, $j \propto r^{1.0}$. This choice is consistent with values found for dark matter haloes within cosmological N-body simulations (Bullock et al. 2001). For simplicity, we initialise the dark matter particles with no net angular momentum. A detailed description of our initialisation method is presented in Kaufmann et al. (2007).

Table 1 summarises the models we explore, but our fiducial runs use $N = 5 \times 10^5$ gas and dark matter particles, and the gravitational softening length is set to be 0.514 kpc. These choices correspond to cases where numerical losses of angular momentum become small (Kaufmann et al. 2007). In Section 5, we perform a number of resolution and convergence tests using lower and higher resolution runs. The low resolution models use $N = 10^5$ gas and dark matter particles. The high-resolution run uses $N = 2 \times 10^6$ particles for each of the species and a softening of 0.257 kpc, scaled as suggested in Zemp et al. (2008). The gas and dark matter particle masses for the three different resolutions are given in Table 1. Finally, we explore two different temperature floors $T_F = 1.5$ and 3×10^4 K. These values alleviate gravitational instabilities in the disc and to crudely mimic the effects of missing heating sources such as those from an

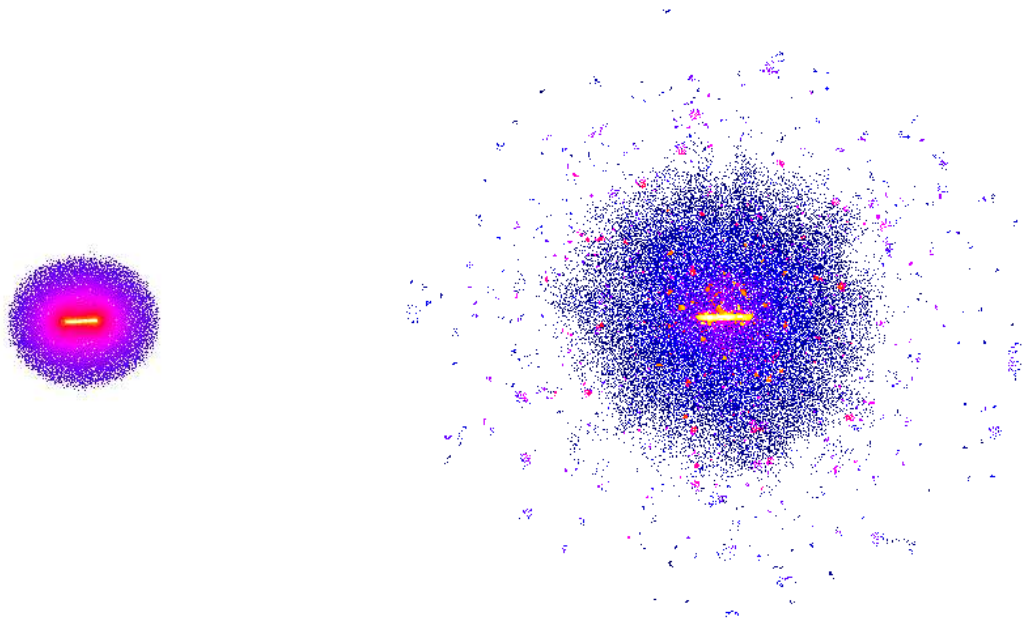

Figure 2. Total 3d gas density after 10 Gyr of cooling for the low entropy case (left side) and the high entropy case (right side). In both cases the box size is 412 kpc. The distribution of halo gas in the two cases is strikingly different. In the low entropy case the gas is highly concentrated within 50 kpc of the disc. For the high entropy run, the gas is spread out much more uniformly at lower density, and dense clumps are clearly seen out to radii of 200 kpc.

ultraviolet background (see e.g. Barnes 2002). They also allow us to explore the properties of fragmentary clouds (e.g., their sizes and neutral fractions) as they are allowed to cool to two different temperatures.

Before exploring the effect of cooling in the simulated haloes, we first allowed them to evolve for 0.5 Gyr with cooling turned off, in order to allow the system to fully relax. Figure 1 shows the density profiles after this initial relaxation phase, before cooling is turned on.

2.2 Hydrodynamics and star formation

We use the parallel TreeSPH (smoothed particle hydrodynamics) code GASOLINE (Wadsley et al. 2004), which is an extension of the pure N-Body gravity code PKDGRAV developed by Stadel (2001). It includes artificial viscosity using the shear reduced version (Balsara 1995) of the standard Monaghan (1992) implementation. GASOLINE uses a spline kernel with compact support for the softening of the gravitational and SPH quantities. The energy equation is solved using the asymmetric formulation, which is shown to yield very similar results compared to the entropy conserving formulation but conserves energy better (Wadsley et al. 2004). The code includes radiative cooling for a primordial mixture of helium and (atomic) hydrogen. Because of the lack of molecular cooling and metals, the efficiency of our cooling functions drops rapidly below 10^4 K. The lack of molecular cooling is unimportant in our investigation because we enforce temperature floors $T_{\rm F} \geqslant 1.5 \times 10^4$ K.

The adopted star formation recipe is similar to that described in Katz (1992); stars spawn from cold, Jeans unstable gas particles in regions of converging flows. The mass of gas particles decreases gradually as they spawn more star particles. Once a gas particle is eligible for spawning stars, it does so based on a probability distribution function with a star formation rate parameter that can be tuned to match the Kennicutt (1998) Schmidt Law. The mass of the gas particles decreases gradually as they spawn more star particles. After its mass has decreased below 10% of its initial value the gas particle is removed and its mass is re-allocated among the neighboring gas particles. Up to six star particles are then created for each gas particle in the disc. For the fiducial and high resolution simulations we allow only one star to spawn per gas particle, thus alleviating the computational load. The subsequent formation of stars has no (energetic) effect to the surrounding gas, i.e., there is no feedback associated with star formation.

2.3 Time evolution and cloud formation

As discussed below, at some point after cooling is turned on in each halo (the time depends on the initial condition), a disc forms in the halo centre. In the low-entropy case, the disc is built from gas that cools rapidly near the halo centre. In the high-entropy case, the disc is built primarily from cool $T \sim T_F$ clouds that condensate within the extended hot halo and fall in to the disc region on ~ 2 Gyr time-scales.

The cool clouds that form in the high-entropy halo arise from a physically expected phenomenon, the thermal instability (most likely as described in Field 1965; see also MB04 and Kaufmann et al. 2006). The thermal instability has less time to develop in the low-entropy halo because the cooling flow is so rapid towards the central region in that case[1].

[1] One of the conditions for cloud formation is that the sound-crossing time, $\tau_\lambda \simeq \lambda_i / v_s$, across a perturbation of wavelength λ_i, should be less than the characteristic cooling time (MB04). If

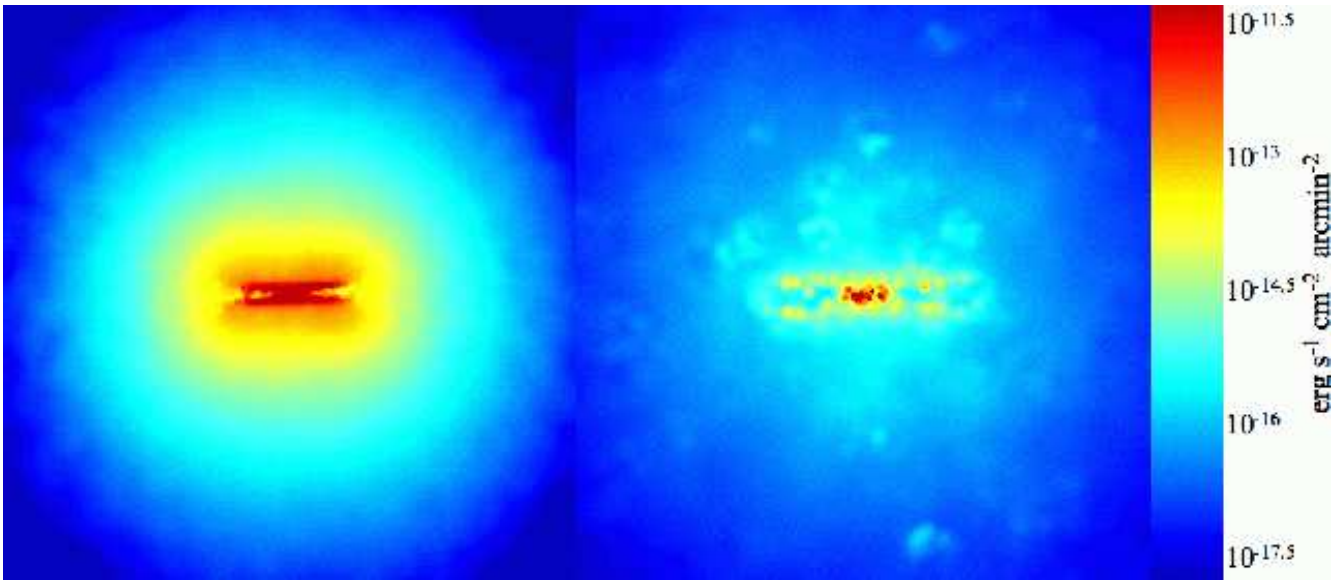

Figure 3. X-ray surface brightness maps of the haloes after 10 Gyr of cooling. The *low-entropy* model is shown on the left and the *high-entropy* model is shown on the right. Boxes are 100 kpc on a side.

However, the fluctuations that seed the thermal instability in our simulations are unphysical. Specifically, the fluctuation field is numerical Poisson noise, and tracks the initial density fluctuations in the SPH particle distribution. Though we expect that real galaxy haloes will have fluctuations in the hot gas distribution, it remains difficult to predict the expected fluctuation field self-consistently from first principles (see MB04). In this sense, our initial (Poisson) fluctuation spectrum may be regarded as an exploratory step towards understanding this complicated problem.

Encouragingly, as we discuss in Section 5, there are many global properties of the simulated gaseous haloes themselves that are robust to the input noise field. While the mass spectrum of fragmentary clouds is sensitive to the initial perturbation spectrum, the integrated mass in cool halo clouds is almost invariant to it. Moreover, the hot gas mass and density profile; the total resultant disc mass; and the time evolution of the system is convergent.

Most importantly, the gross difference between the high-entropy halo (which produces clouds) and the low-entropy halo (which does not) is also a physical difference – the initial fluctuation amplitudes in the high-entropy and low-entropy haloes are very similar (Section 5). We defer the somewhat lengthy discussion of the cloud property dependence on resolution and on other physical processes in Section 5.

this condition is not satisfied the perturbation is erased because the local cooling time is too close to the mean cooling time and the whole region becomes isothermal. While roughly the same level of perturbations are resolved in the low and high entropy simulations and the sound speed ($v_s \propto \sqrt{T}$) remains comparable, the cooling time in the centre of the low entropy halo is much shorter due to the higher gas density as well as a lower initial temperature and its perturbations get erased. The cooling time in the high entropy case is also longer because the cooling rates for primordial gas drop from $T \sim 4 \times 10^6$ K to $\sim 10^6$ K (Katz et al. 1996), whereas the low entropy halo starts in the rising part of the cooling curve, see Figure 6.

3 THE RESULTING HALO GAS

First we focus on the simulation results after 10 Gyr of cooling. Figure 2 shows images of the 3d gas density for each case, and illustrates that the two scenarios create strikingly different gas halo distributions. In the left panel, we see that the low-entropy halo has cooled to form a central disc and that the gas density is quite high only in the central disc region. The high entropy halo (right) has produced a disc that is less massive (see below) along with an extended ~ 200 kpc distribution of fragmented, cool $T = T_F \sim 10^4$ K clouds. The total cool mass that resides in the final high-entropy halo is $\sim 5 \times 10^9\, M_\odot$ after 10 Gyr of evolution (see Table 2). In contrast, the low entropy case (left) yields virtually no extended distribution of cool clouds in the halo. It is clear then that the initialised differences in the gas profiles persist and result in striking differences after 10 Gyr of cooling. This suggests that observations of the gaseous haloes of galaxies can be used to understand their cooling history. Below we discuss these results in the context of observational signatures.

3.1 X-ray observations

Figure 3 shows X-ray surface brightness maps for each halo after 10 Gyr of cooling. The X-ray emissivities were calculated in the 0.1 to 10 keV band using the MEKAL software package[2] assuming a hot gas metallicity of 0.3 solar. As mentioned in the section 1, some observations suggest an upper limit for X-ray emission from disc galaxies of $S_x < 10^{-14}$ erg cm^{-2} s^{-1} arcmin^{-2} (Pedersen et al. 2006). The emission of the hot halo in the low entropy run is up to ~ 100 times too bright in the X-ray, while the high entropy case is within these observational bounds.

[2] see http://heasarc.gsfc.nasa.gov/docs/xanadu/xspec/

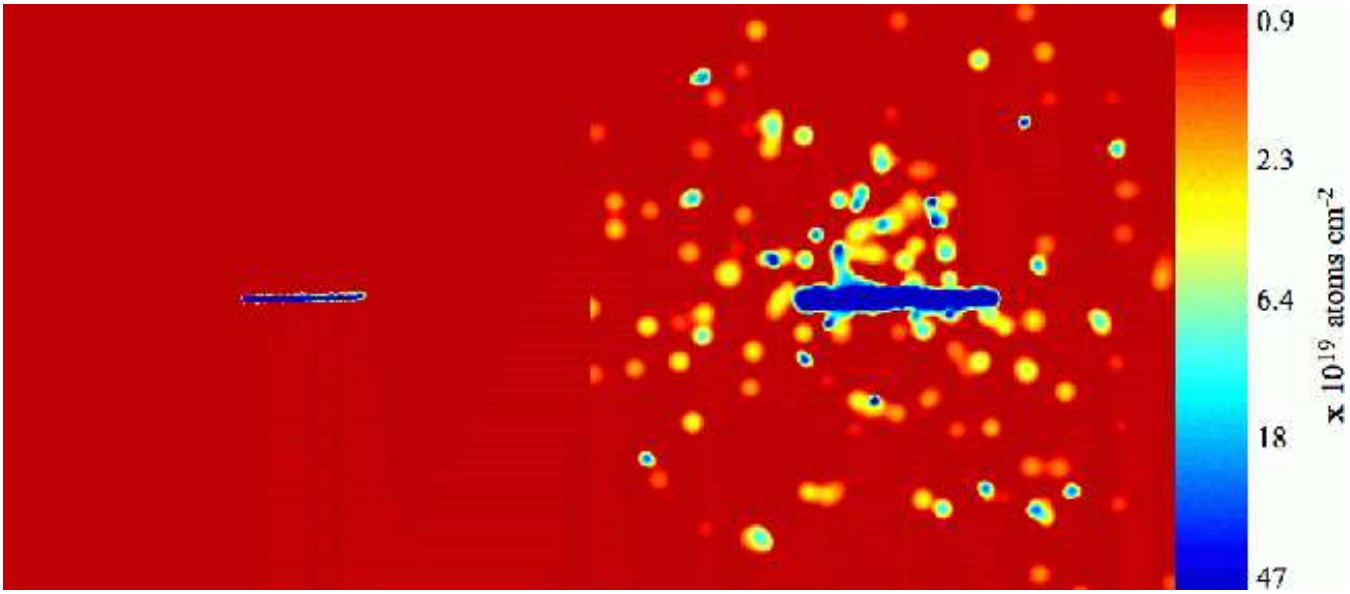

Figure 4. Maps of the projected HI density for the low-entropy case (left) and high entropy case (right). Shown is the case for $T_F = 15\,000$ K, see text for details. Boxes are 100 kpc on a side.

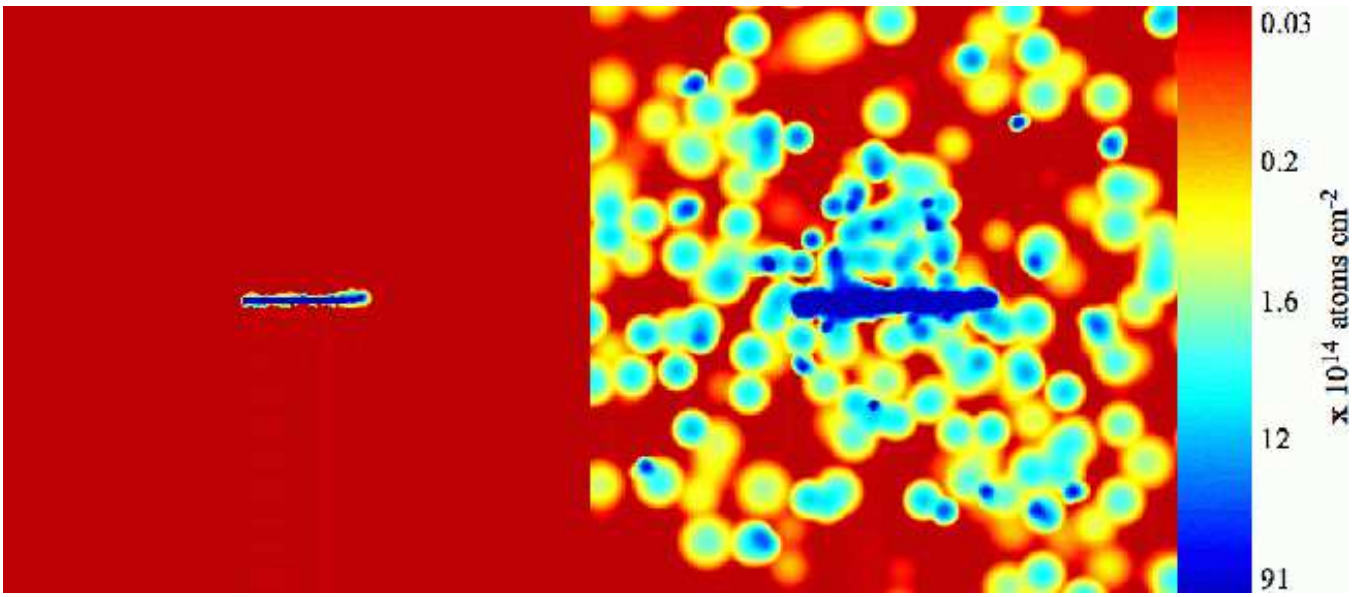

Figure 5. Maps of the projected Mg II density for the low-entropy case (left) and high entropy case (right). Shown is the case for $T_F = 15\,000$ K and 0.3 metallicity gas, see text for details. Boxes are 100 kpc on a side.

Benson et al. (2000) reported limits on the X-ray luminosities of three galaxy halos of $L_X < 0.4$, 1.2 and 3.8 $\times 10^{41}$ erg s^{-1}. In this investigation, the authors did not include luminosity from the central disk region in order to concentrate on halo gas explicitly. In Table 2 we list the L_X values for each of our halos, excluding the central 10 kpc region by analogy with Benson et al. (2000). The luminosity from the the high entropy model ($L_X = 2.2 \times 10^{39}$ erg s^{-1}) is well below the observed limits, while the value for the low entropy model ($L_X = 1.3 \times 10^{41}$erg s^{-1}) is inconsistent with two of the halo L_X limits from Benson et al. (2000).

Finally we note that even our high-entropy halo is too bright in the X-ray in the very central disk region. Unfortunately, the predicted luminosity in this region suffers from both numerical limitations and from the lack of important feedback physics, which almost certainly is important on this scale. First, at the disc-halo interface, the densities of the hot gas particles and therefore their X-ray emission are over-estimated due to the SPH smoothing procedure[3]. Furthermore, feedback from star-formation is expected to modify the thermal structure of the hot halo at the disc-halo

[3] However, one can show that if the cold gas particles are cut away and the densities of the remaining gas particles are then recalculated, the X-ray luminosities will be underestimated (Toft et al. 2002)

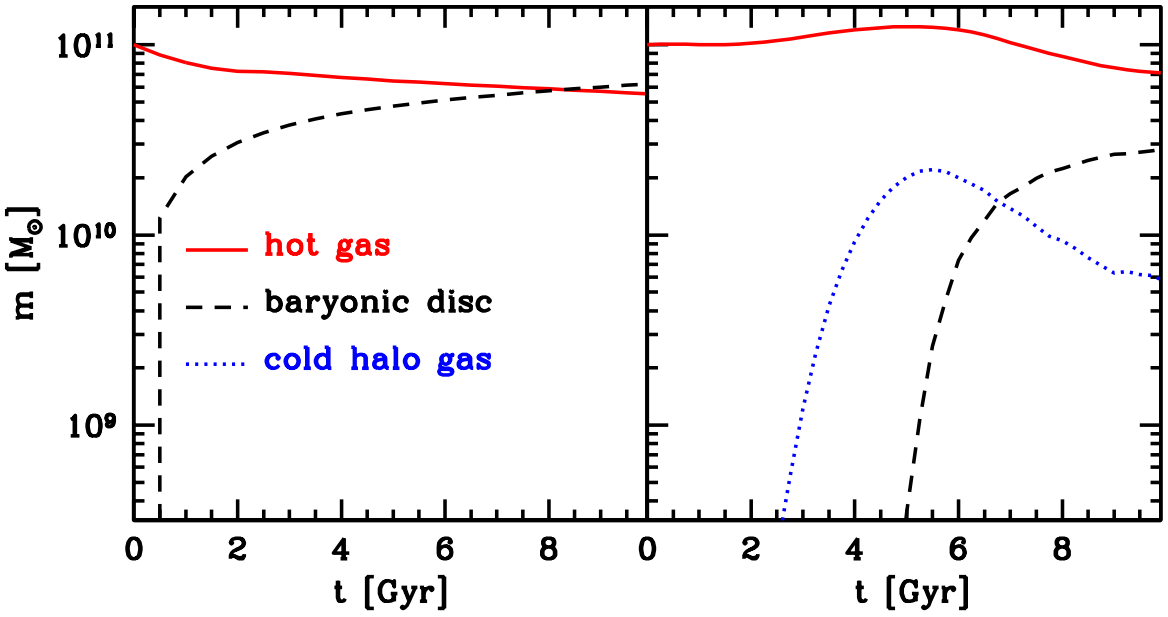

Figure 7. Mass evolution of the different gas phases, **left** low entropy and **right** high entropy model. Note, that the low entropy model does not show a significant amount of cold halo gas.

interface and this could act to lower the cooling rate there. If we blindly calculate the X-ray luminosity that comes from the central 10 kpc region we find $L_X(< 10\mathrm{kpc}) = 2.9 \times 10^{41}$ erg s^{-1} for the high entropy model and 2.0×10^{43} erg s^{-1} for the low entropy model. The latter is almost four orders of magnitude higher than the measurement of Li et al. (2008) who find a total X-ray luminosity from the central part NGC 5775 to be $\sim 3.5 \times 10^{39}$ erg s^{-1}. Realistic comparisons to these observations must be deferred until more accurate simulations are run, but it would seem difficult to reconcile a factor of ten thousand disagreement, as is seen with the low-entropy model.

3.2 Cool-gas observations

As discussed in Section 5, the cloud mass spectrum is sensitive to the initial fluctuation field, therefore our results in this section should be regarded as an exploration of the expected trends rather than detailed first-principle predictions. Nonetheless, we expect the differences between the high-entropy and low-entropy cases to be robust.

The H I HVCs in the Galactic halo are potentially building up the baryonic mass of the Galaxy (Putman 2006). To compare with observations of the local HVC population, we derived the neutral H I fraction of the cold material using Cloudy (version C06.02), last described by Ferland et al. (1998). The chosen radiation field will influence the H I fraction heavily but several observations suggest that extragalatic ionizing photons are likely the source of the ionisation (see e.g. Maloney 1993), so we adopt the metagalactic background spectrum of Sternberg et al. (2002), which covers wavelength from infrared to X-rays. The ionizing photons are mainly produced by quasars and star-forming galaxies. The influence of radiation from the Galaxy is smaller: Assuming a small but very uncertain escape fraction of the Lyman continuum flux (contributed mainly by the OB associations), $f_{esc} \sim 5\%$ (e.g., Dove, Shull, & Ferrara 2000), the metagalactic contribution dominates over the Galactic one at a distance of ~ 180 kpc. For soft X-ray photons, the two contributions equal at ~ 16 kpc (Slavin, McKee, & Hollenbach 2000). A variation of the ionizing flux by a factor of 2 may affect the estimation of the gas mass by a factor of 1.5 (Maloney & Putman 2003).

The amount of neutral H I in the simulations depends also critically on the temperature of the cold clouds (which have cooled down to the temperature floor set in the simulation). The 30 000 K temperature floor prevents the formation of a large amount of neutral H I, the large core model predicts $\sim 1.5 \times 10^6\ M_\odot$ of neutral H I distributed in the halo (out to 200 kpc). But (background) radiation from stars and cosmological sources might not be able to keep the gas as hot. We checked that dependence by evolving the two fiducial models further for 40 Myr with a temperature floor of 15 000 K; the neutral H I mass in the halo is then $\sim 9 \times 10^8\ M_\odot$ for the high entropy model: this is an increase of more than a factor 100, which demonstrates how sensitive the H I fraction is to the temperature of the cool clouds.

The high entropy case with a temperature floor of 15 000 K is in fairly good agreement with the observations of the Milky Way. Putman (2006) estimated the total gas mass in the HVCs of the Milky Way to be $1.1 - 1.4 \times 10^9\ M_\odot$, if assuming the clouds are distributed within 150 kpc. Our prediction is somewhat higher ($5.5 \times 10^9\ M_\odot$, Table 2), but the estimated total gas mass in the observed HVCs would increase if their average distance is somewhat higher and/or their H I fraction is lower than assumed (Putman 2006).

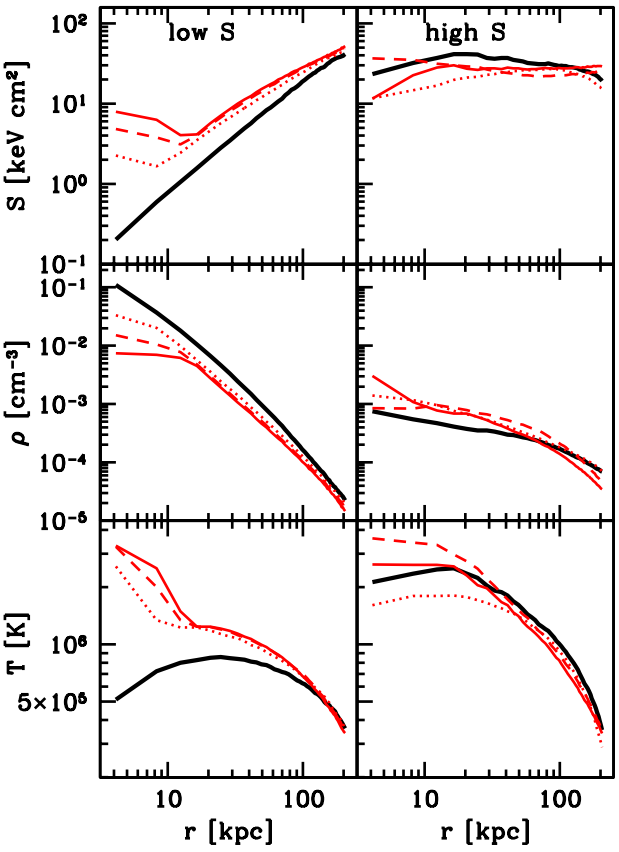

Figure 6. Evolution of entropy (top), density (middle) and temperature (bottom) of the hot gas for the low entropy (left) and high entropy (right) models. The lines represent 0 (thick solid), 3 (dotted), 7 (dashed) and 10 (solid) Gyr of cooling. In the low entropy case the entropy increases in the centre of the halo as the lowest entropy material cools out and the average temperature of the hot gas increases. The density profile monotonically decreases and a small core in the hot gas starts to form. In the high entropy case the entropy, the density and the temperature oscillate around the original values with little evolution. *A hot gas halo that has this profile can remain in a steady state for 10 Gyr.*

The velocity field of the simulated clouds is quite similar to the one of observed HVC's, but since it is dependent on the initial spin of the hot gas and initial noise field, we defer a detailed comparison.

The choice of 15 000 K for the high entropy model also agrees quite well with observations of the H I mass in the nearby massive spiral NGC 891, for which Sancisi et al. (2008) quote an H I mass in the halo of $\sim 1.2 \times 10^9\,M_\odot$. Those authors also infer a mean "visible" accretion rate of cold gas in galaxies to at least $0.2\,M_\odot\,yr^{-1}$; today's rate for the high entropy model can be estimated by multiplying the total mass accretion rate to the disc at the final time step ($2.05\,M_\odot yr^{-1}$) with the fraction of cold accretion (0.75) and the H I fraction (0.18). The visible accretion rate in the large core model is therefore $\sim 0.28\,M_\odot\,yr^{-1}$. Rand & Benjamin (2008) found less H I ($\sim 10^8\,M_\odot$) around NGC 5746, a edge-on galaxy known to have a large corona. The radiation field around that galaxy might be somewhat higher, preventing some H I to form, and the cool clouds stay more ionised as expected in the case of a temperature floor higher than 15 000 K. The covering fraction for H I with number densities $N(H\,I) > 2 \times 10^{18}\,\mathrm{cm}^{-2}$ is approximately 35% in the high entropy simulation similar as that found around the Galaxy (Murphy, Lockman & Savage 1995).

The low entropy model does not show any neutral H I outside of the disc for either temperature floor. While Figure 4 illustrates the situation with the lower temperature floor, the derivation of self-consistent H I masses would require a simulation, which follows the feedback from the radiation field from stars and background sources self-consistently. The values given above are likely bracketing the expected H I masses but they also show, that the H I clouds are always embedded in substantial clouds of ionised hydrogen. Furthermore, a galactic fountain - not yet included in the simulations - might produce more extra-planar gas (Fraternali & Binney 2008).

We also calculate the Mg II ionisation fraction using CLOUDY, and estimate the covering fraction of the Mg II gas clouds (see the maps in Figure 5 and summary in Table 2). Again, the covering fraction given by the high entropy case with temperature floor of 15 000 K, ~ 0.6, is consistent with observations. For ~ 20 galaxies, Tripp & Bowen (2005) found a Mg II covering fraction of ~ 0.5, whereas Chen & Tinker (2008) report a Mg II covering fraction of ~ 0.8. Bechtold & Ellingson (1992) reported a smaller cover fraction, ~ 0.25, but they observed within a bigger impact distance, $D \leqslant 85$ kpc.

In summary, the high entropy model can reproduce almost all of the observed qualitative features of halo gas. The differences between the high and low entropy models in their X-ray luminosities are particularly striking and should be robust to numerical uncertainties.

The high-entropy model is also able to reproduce observed covering fractions for absorption systems. However, the predictions depend sensitively on the temperature floor adopted (which acts as a proxy for the external ionizing field) and, as mentioned earlier, on the initial (unphysical) noise field in the simulations. Nonetheless, for the same initial noise field, the high-entropy model facilitates the formation of fragmentary clouds while the low-entropy model does not. Specifically, the low-entropy model has no cool halo clouds to be seen as high velocity clouds or quasar absorption systems, while the high-entropy model allows the clouds to emerge over time-scales that are longer than the inflow time-scale associated with cooling from the central region.

4 THE TIME EVOLUTION OF THE HOT GAS HALO AND THE GALACTIC DISC

Figure 6 illustrates the evolution of the hot gas ($T > 50\,000$ K) density profiles (middle), temperature (lower) and entropy profiles (upper) for each of our initial haloes (the low and high entropy models are shown in the left and right panels, respectively). It is clear that the different initial gas distributions lead to a completely different cooling behaviours. The low entropy halo cools quickly from the central region. Over the same period, the hot gas density of the high entropy

model remains remarkably stable and the entropy profile remains quasi-stable, but does experience some oscillations. We show in Section 5 that these results are stable to numerical convergence.

The build up of the disc and cold gas populations in both scenarios can be seen in Figure 7, which shows the mass evolution in the central disc galaxy (dashed), and the hot halo component (red, solid) as a function of time. The hot gas includes all $T > 50,000$ K gas within the halo virial radius. In the low entropy case, the hot gas quickly cools within a ~ 2 Gyr to form a massive disc ($2\times10^{10}M_{\odot}$). Then cooling proceeds at a slower rate with the hot halo being depleted and the disc growing larger to $6\times10^{10}M_{\odot}$ after 10 Gyr. In contrast, in the high entropy case, no cooling occurs for the first ~ 2 Gyr. Then the hot gas starts to fragment into cool clouds that are embedded within the hot halo (blue dotted line) which eventually fall in to form a central disc[4]. Note that the halo cloud population peaks with a total mass of $2\times10^{10}M_{\odot}$ before a central disc starts to form. The hot gas in this case shows a slight increase in mass at ~ 3 Gyr as hot gas enters the halo from beyond the virial radius. A similar upturn is not seen in the low entropy case because the gas always cools faster than new gas enters the halo virial radius.

The final disc in the high entropy case is significantly less massive $\sim 3\times10^{10}$ $M_{\odot}$ and also has $\sim 60\%$ more specific angular momentum than in the low entropy run (see Table 2). The reason for this is that the disc is build up not only from gas cooling close to the centre of the halo and getting incorporated to the disc but also from material which cooled already far away from the central disc. Roughly 45% of the material that makes the disc in the high entropy halo is accreted as cool clouds that formed beyond 30 kpc from the disc. Note that, while the total angular momentum of the gas in the two simulations was the same initially, the discs form out of different portion of the specific angular momentum distribution.

These trends can be clearly understood by looking at the energy of the hot gas (Figure 8). The low entropy run loses most of its energy early on while the energy losses of the high entropy run are quite modest over the 10 Gyr. Note that, although the low and high entropy runs are losing energy at a similar rate from 6 Gyr on, their X-ray surface brightness emission (Figure 3) is very different due to different spatial distribution of the cooling — the low entropy run cools in the centre whereas cooling in the high entropy run is diluted in the whole halo.

Interestingly, the radial scale-length and the specific angular momentum of the disc after 10 Gyr is larger in the high entropy run than in the low entropy run. This shows, that even though the cool clouds might lose angular momentum due to ram pressure while sinking to the centre, this path of disc formation actually increases the angular momentum content by more than 50% compared to the low entropy disc (Table 2), possibly relieving the "angular momentum problem" in disc formation.

[4] The time evolution beyond 10 Gyr showed, that the density profile in the high entropy case remained relatively stable and the mass growth of the galactic disc slowed down compared to the period from 5 to 10 Gyr.

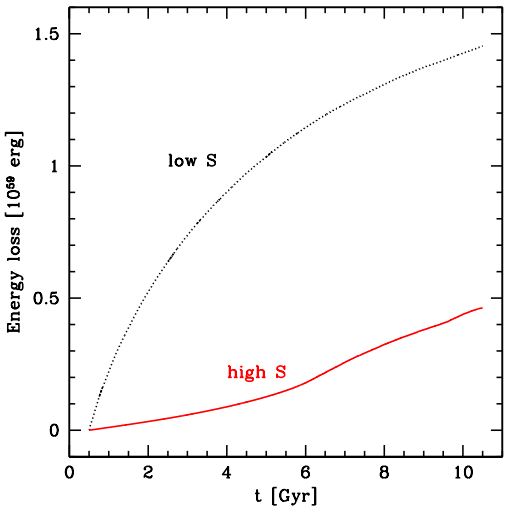

Figure 8. The time evolution of the total energy loss of the system is shown. Cooling is much more efficient in the low S model compared to the high S simulation.

Besides producing a gas halo that agrees with observations it appears that the high entropy simulation is also able to create a disc galaxy that does not suffer from the common problems associated with disc galaxy formation in numerical simulations. The reduction in disc mass and increase in specific angular momentum suggests that building discs from cool clouds is a promising path.

5 RESOLUTION TESTS AND EXPLORATION OF COOL CLOUD PROPERTIES

We have conducted resolution tests in our high-entropy halo by increasing the number of gas particles within the virial radius from 10^5 to 2×10^6 in a series of three simulations (see Table 1). While the cool clouds that form in these simulations arise from a real, physical process that amplifies initially small perturbations (the thermal instability) the initial seed perturbations are not physically motivated. Specifically, they are set by Poisson sampling noise (Kaufmann et al. 2006). Therefore, the noise field that arises from our sparse sampling statistics may be regarded as a toy model example of the fluctuation field that is expected to exist in real galaxy haloes (see MB04 for a discussion). Unfortunately, the true nature of the expected perturbation spectrum will likely remain difficult to predict from first principles for many years. This motivates us ask whether there are quantities that remain invariant to different perturbation distributions.

We would like to determine whether our ignorance associated with the expected perturbation field prohibits us from predicting any generic features of the cooling haloes. As we now describe, we find perhaps the most encouraging result possible: most global properties of the resultant haloes (including the integrated mass in cool halo material and the radial extent of this cool halo gas) are robust to the initial noise field. The initial fluctuation spectrum seems to affect only the resultant cloud mass spectrum. Of course, the latter fact implies that the cloud mass spectrum and related quantities like cloud covering factors are subject to

Table 2. Various results for the fiducial models after 10 Gyr

model	high S	low S
(1a)* H I cloud mass in $M_\odot$ at 15000K	9×10^8	0
(1b)* H I cloud mass in $M_\odot$ at 30000K	1.5×10^6	0
(2a)* H I covering fraction at 15000K	0.36	0.01
(2b)* H I covering fraction at 30000K	0.00	0.00
(3a)* Mg II covering fraction at 15000K	0.60	0.01
(3b)* Mg II covering fraction at 30000K	0.02	0.00
(4) total cold halo gas in $M_\odot$	5.5×10^9	0
(5) total hot halo gas in $M_\odot$	7.1×10^{10}	5.5×10^{10}
(6) total disc mass in $M_\odot$	2.9×10^{10}	6.3×10^{10}
(7) disc scale length in kpc	3.6	2.6
(8) disc j in kpc km s^{-1}	740	468
(9) L_X in erg s^{-1}	2.2×10^{39}	1.3×10^{41}

(1) Total H I mass in the halo, see section 3.2.
(2) Covering fraction for $N(H\,I) > 2 \times 10^{18}\,cm^{-2}$ within a box of 100 kpc for, see section 3.2.
(3) Covering fraction for $N(Mg\,II) > 10^{13}\,cm^{-2}$ within a box of 100 kpc for, see section 3.2.
(4) Cold gas within the virial radius, without the gaseous disc.
(5) Hot gas within the virial radius.
(6) Total disc mass including gas and stars
(7) Radial scale length of the stellar disc measured by fitting an exponential to the surface density profile neglecting the bulge region.
(8) Specific angular momentum of stars plus cold gas disc.
(9) Bolometric X-ray luminosity within a 100 kpc box around the disc for a metallicity of 0.3 solar. A 10 kpc box around the centre of the disc has been cut out, see section 3.1.
* Number so marked is dependent on the initial noise field in the simulation and is presented to guide expectations and to contrast results between the two initial setups.

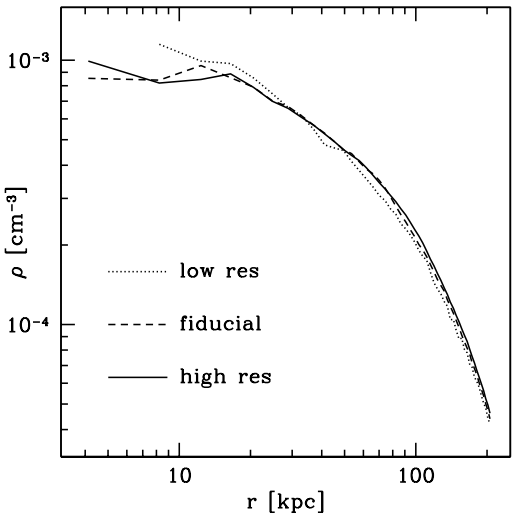

Figure 9. The hot gas density of the high entropy model after 7 Gyr of evolution at different resolutions: The profile remains basically unchanged for an increase of a factor 20 in particle number.

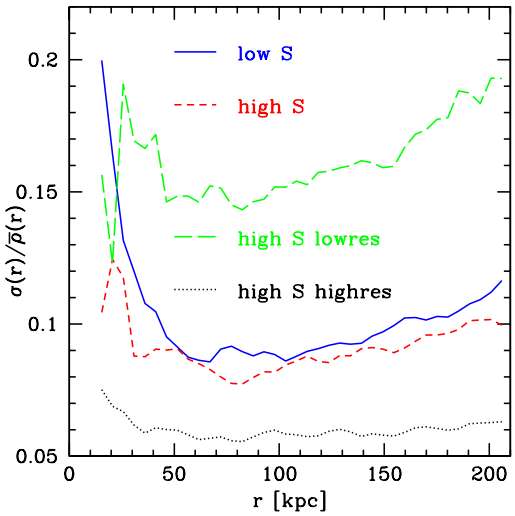

Figure 10. Comparison of the perturbations in the gas density after the evolution with an adiabatic EOS. The RMS density fluctuation divided by the mean density in that radial bin is plotted versus radius (the local density was smoothed over the same mass for the different resolutions).

very large uncertainties. There is hope that the 'real' fluctuations can be modeled effectively in very high resolution cosmological simulations, but disentangling these expected fluctuations from numerical noise will be a difficult task. Even in cosmological simulations, it may be best to concentrate on robust, global quantities, like the integrated mass, at least in the near future.

Figure 9 shows that the hot gas density profile of the the high entropy model is convergent after 7 Gyr at different resolutions. Therefore, the fact that a quasi-stable hot gas halo can exist over a significant fraction of the Hubble time holds at all the resolutions tested. Moreover, the integrated mass and radial extend of cold halo gas (the total mass in halo clouds) is also convergent over these three cases, as summarised in Table 3. We also have run one lower resolution simulation for the low-entropy case (with 10^5 gas particles, see Table 1) and find that the global results for this case are almost identical to the higher resolution run.

5.1 Cloud Properties: Resolution and Temperature Floor Tests

We identify clouds using a friends of friends algorithm (FOF) with 32 particles as the minimum threshold (equal to the number of particles in the smoothing kernel). The linking length was chosen to be 0.2 times the mean particle separation, and we checked in the standard simulation that the number of clouds found with the FOF depends only weakly on the exact choice of the linking length. We note that we have additional diffuse, cool material in the halo that cannot be identified or resolved by our 32 particle FOF algorithm. This additional material is included in our accounting of total 'cool halo gas'.

We expect that the resultant cloud mass spectrum will depend on the level of initial density perturbations, and hence on the resolution. Figure 10 shows an illustration of the initial RMS density fluctuations as a function of radius for the standard-resolution high-entropy and low-entropy runs before cooling is turned on (i.e. after the 0.5 Gyr of

evolution with an adiabatic EOS). Specifically, we measure the RMS density variation around each particle at radius r using the nearest $n = 32$ particles (the number used in the smoothing kernel of the simulations) to calculate its local density, compared to the mean density averaged in the respective radial bin. We see that the noise level is comparable between the two simulations (and even slightly larger in the low-entropy case). This demonstrates that it is not a difference in the initial perturbations that gives rise to the formation of clouds in the high-entropy run, but rather the difference in the initial density profiles.

Figure 10 also shows the fluctuation amplitude for the lower and higher resolution realisations for the high-entropy case (where here the value of n in the measurement is adjusted to $n = 6$ and $n = 128$ respectively so that the total mass averaged over remains fixed). The noise level varies as expected from Poisson statistics. The resulting cloud mass functions for the three high-entropy runs are shown in Figure 11. We find that when the initial fluctuation amplitude is smaller (from higher particle number) the spectrum of cloud masses is correspondingly reduced (as $\sim 1/\sqrt{N}$ in the particle number). Thus any prediction that depends on the mass spectrum of clouds, including cloud sizes and covering fractions, will require an understanding of the initial perturbation spectrum. We note that it has been shown (Kaufmann et al. 2006, their Figure 12) that if the level of perturbations is kept fixed while increasing particle resolution, the resultant cloud spectrum is independent of particle number (down to the resolution limit) therefore the noise spectrum itself is the critical unknown quantity in these simulations. Though the mass spectrum of clouds does not converge, we find that the total cool mass in the halo and its radial extent in the large core simulation is fairly independent of the numerical resolution, even for an increase of the number of gas particles by a factor of 20, see Table 3.

We find that global differences due to using a different temperature floor are small. Clouds do cool down to the respective temperature floor imposed, so heating by the clouds motion through the hot background is either not important or not captured by the code. The spatial and the velocity distribution of the clouds after 7 Gyr in the high entropy LT run with $T_F = 15\,000$ K are comparable to the fiducial run at $T_F = 30\,000$ K. On the other hand, the densities of the clouds in the LT run are increased due to the smaller internal pressure, as expected. Nonetheless, the exact value of the lowest temperature imposed is not of critical importance for the total mass in clouds. However, it is very important for the H I mass fraction in each cloud (and in the expected covering fraction) as discussed in Section 3.

5.2 Evolution and dissolution of the clouds

After 6 Gyr of evolution of the high entropy high-resolution run, a variety of cool clouds (temperature equal to the cut-off temperature in the cooling function, $T_F = 30\,000$ K in most cases) are found, ranging from compact clouds close to the disc (with masses $\sim 10^6 - 10^7$ and sizes of $r_{cloud} \sim 0.7 - 1.3$ kpc) to diffuse clouds in the outer halo (typical masses of $\sim 10^7$ M$_\odot$ and larger sizes of $r_{cloud} \sim 4.5$ kpc). Clouds sizes are set by pressure confinement, therefore at fixed mass they are more diffuse at large radius, where the background hot gas pressure is lower. Because of the increased hot gas density towards the halo centre, we can resolve lower mass clouds more easily near the disc.

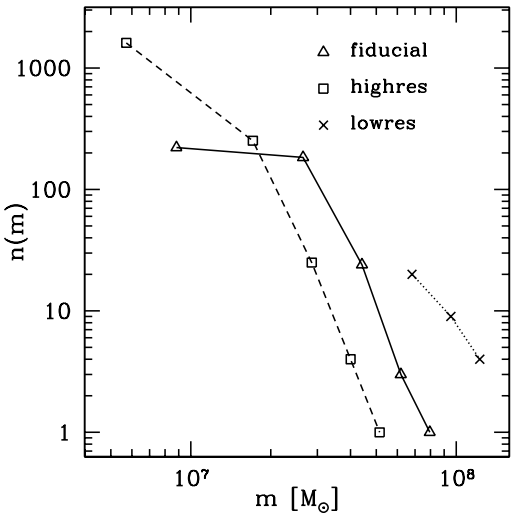

Figure 11. Cloud mass spectra for the high entropy run at different resolution (fiducial, low-res and high-res) after 6 Gyr of evolution with cooling. Note, that even the most massive clouds in the low-res run do not contain more than a hundred particles.

Table 3. Convergence Test Results for high-entropy case. Listed are properties of the cold gas within $R_{200} = 206$ kpc after 7 Gyr of cooling.

(1) Name	(2) Radius [kpc]	(3) M_{cold} [$M_\odot$]	(4) M_{halo} [$M_\odot$]
high entropy low-resolution	$\sim R_{200}$	2.9×10^{10}	1.2×10^{10}
high entropy	$\sim R_{200}$	3.0×10^{10}	1.4×10^{10}
high entropy high-resolution	$\sim R_{200}$	3.0×10^{10}	1.4×10^{10}

(2) Distance out to which cold particles can be found.
(3) Total cold mass (includes stars).
(4) Total cold gas mass in the halo, excluding the disc.

The fate of fragmentary clouds depends on various mechanisms (see also Kaufmann et al. 2006, MB04). One of the most important processes that influences cloud survival is the Kelvin-Helmholtz (KH) instability. As a cool, dense cloud moves through a hot, tenuous background, the interface between the two phases is subject to the growth of this instability, which can disrupt the clouds. At our resolution, the standard implementation of SPH does not resolve such instabilities due to smoothing and the artificial viscosity which tends to blur any sharp interface between the inner and outer medium (Agertz et al. 2007). For the case in which self-gravity is unimportant, Murray et al. (1993) derive a characteristic growth time for the instability of

$$\tau_g \approx \frac{r_{cloud}(\rho_{cloud}/\rho_{bg})^{0.5}}{U}, \quad (1)$$

where U is the relative velocity and ρ_{bg} is the density of the background medium. The clouds are therefore expected to break up on time-scales comparable to τ_g. In their numerical experiments they actually found that the mass loss was

still quite small over time scales twice as long as τ_g. In our simulations the density contrasts range from ~ 10 to ~ 300, the relative velocities U from ~ 50 to ~ 160 km/s and therefore we end up with τ_g ranging from ~ 0.3 to ~ 0.07 Gyr. Based on these estimates, the KH instability could dissolve a significant fraction of the clouds with the parameters given above, if they were evolved in isolation. But Vietri et al. (1997) showed that with the inclusion of radiative cooling the effect of the Kelvin-Helmholtz instability are stabilised and clouds in the mass range given above survive. Moreover, Vieser & Hensler (2007) showed that the destructive effect of KH instability is significantly slowed if heat conduction is included. We also note that the thermal instability can be suppressed by buoyant oscillations in a medium with a pressure gradient in thermal equilibrium (Balbus & Soker 1989). However our simulations (and real gaseous galactic haloes, for that matter) are not in thermal equilibrium. This suppression is also reduced if convection occurs in the gas.

Clearly, the issue of cloud survival remains an important one, especially for questions to do with the manner of gas feeding onto galaxies. The situation in simulations is more dynamical than accounted for in most analytic explorations of KH: clouds grow by merging and new clouds are born due to the thermal instability. Taken the Kelvin-Helmholtz instability together with conductive evaporation, which can prevent the survival of small clouds (see MB04), these effects would reduce the total mass in cool halo gas by destroying the smallest clouds and modifying the outer layers of the bigger clouds in our simulations[5]. Interestingly, however, for the problem of over-cooling in galaxy haloes, the disruption of cool clouds back into the hot halo can do nothing but help.

In summary, the cool cloud mass spectrum that feeds disc formation is dependent on a variety of physical processes: hydrodynamical instabilities, conduction and the radiation field, none of which are currently resolved in these simulations (or any other cosmological simulations). The initial cloud mass spectrum is determined by the initial perturbation spectrum, which is difficult to determine from first principles. Encouragingly, however, we find that the total amount of gas that cools into clouds seems to be independent of the initial perturbation spectrum. The results we have presented on cloud properties can be seen as an upper limit on the total mass of cool clouds as most unresolved processes destroy clouds. The details of how the clouds would be observed is unfortunately more complicated because it depends on the temperature of the gas in the clouds and the ionizing background.

6 SUMMARY AND CONCLUSIONS

We studied the cooling flow of gas within equilibrium NFW dark matter haloes, in order to mimic the expected growth of $10^{12} M_\odot$ halo galaxies after the cold-flow, rapid accretion period has ended for these systems ($z < 1$). The two simulations contained the same baryonic mass and were identical other than their initial gas density profiles – one with a low central entropy that tracked the NFW density profile of the dark matter, and one with a high central entropy and low-density core in its density profile as might be expected in models with substantial pre-heating feedback. The simulations show dramatic differences in their subsequent evolution. The high-entropy gas halo forms a fairly low-mass disc with high angular momentum content, an extend halo cloud distribution, and an extended hot gas halo that produces an X-ray surface brightness consistent with observations. Most of the baryons in this case reside in the hot, quasi-stable gas halo. In contrast, the low entropy run forms a smaller, but heavier disc quickly, shows no H I in the halo, and has an X-ray luminosity that greatly exceeds observed limits for normal spiral galaxies. These results have led us to three main conclusions:

- Changing the distribution of hot gas around galaxies, as might be expected in some pre-heating feedback schemes, dramatically alters many aspects of the subsequent cooling behaviour, as well as the energy required to stabilise the systems to subsequent cooling (see also Mo & Mao 2002; Oh & Benson 2003). These differences are not only manifest in the resultant optical characteristics of the central disc galaxy, but they may be tested via X-ray observations and other non-optical probes of the haloes themselves.
- Galaxy formation that proceeds via the thermal instability and cloud infall can dramatically affect the properties of the resultant galaxy system. In our high entropy simulations, the resultant disc is not only less massive, but it is larger, with more specific angular momentum than in the low-entropy case. Such behaviour is simply not possible if the cooling occurs mainly near the disc in a central cooling flow.
- It is possible to maintain a high-mass ($M \sim 5 \times 10^{10} M_\odot$), low-density, quasi-stable gaseous halo around a Milky Way size galaxy for a significant fraction of the Hubble time without a continuous input of feedback energy. Such an extended halo (once in place) is a much better match to observations than low-entropy (cuspy/high-density) hot gas haloes that are commonly adopted in first-order analytic explorations.

These simulations show that the large core initial gas density profile without any feedback can produce a galaxy that hardly suffers from many of the classical problems in galaxy formation. Kereš et al. (2009) have seen (smaller) cores in the density profiles in some of their cosmological haloes and speculate that they could be produced during the early chaotic, rapid assembly phase of haloes (without the need of AGN heating or other preventive feedback). Another possibility, explored by Tang et al. (2008) using one-dimensional simulations, is that AGN pre-heating is triggered by the initial galaxy collapse itself. This latter collapse could be associated with the end of the cold-mode phase (Kereš et al. 2009) or (perhaps equivalently) the end of the rapid accretion epoch (Wechsler et al. 2002). As we have shown, once the hot gas density profile is suitably rearranged, it basically shuts down associated hot halo cooling for several Gigayears without any further input of energy after that early phase. Tests of these ideas using high resolution numerical simulations in a full cosmological set-up are underway.

[5] See also Kaufmann et al. (2006) for a discussion on cooling below 10^4 K and self-shielding effects.

ACKNOWLEDGMENTS

The numerical simulations were performed on the IA64 Linux cluster at the San Diego Supercomputer Center. We would like to thank Stelios Kazantzidis for providing a code to generate isolated dark matter haloes. We acknowledge useful and stimulating discussions with Andrew Benson, Hsiao-Wen Chen, Chris Churchill, Avishai Dekel, Jana Grcevich, Dusan Kereš, Lucio Mayer, Julio Navarro, Peng Oh, Josh Peek, Mary Putman, Jesper Rasmussen and Joop Schaye. This work was supported by the Center for Cosmology at UC Irvine. TK has been supported by the Swiss National Science Foundation (SNF).

REFERENCES

Agertz, O., et al. 2007, MNRAS, 380, 963
Balbus, S. A., & Soker, N. 1989, ApJ, 341, 611
Barnes, J. E., 2002, MNRAS, 333, 481
Balsara, D. S. 1995, Journal of Computational Physics, 121, 357
Bechtold, J., & Ellingson, E. 1992, ApJ, 396, 20
Benson, A. J., Bower, R. G., Frenk, C. S., & White, S. D. M. 2000, MNRAS, 314, 557
Benson, A. J., Bower, R. G., Frenk, C. S., Lacey, C. G., Baugh, C. M., & Cole, S. 2003, ApJ, 599, 38
Birnboim, Y., & Dekel, A. 2003, MNRAS, 345, 349
Bower, R. G., Benson, A. J., Malbon, R., Helly, J. C., Frenk, C. S., Baugh, C. M., Cole, S., & Lacey, C. G. 2006, MNRAS, 370, 645
Bregman, J. N., & Lloyd-Davies, E. J. 2007, ApJ, 669, 990
Brooks, A. M., Governato, F., Quinn, T., Brook, C. B., & Wadsley, J. 2009, ApJ, 694, 396
Bullock, J. S., Dekel, A., Kolatt, T. S., Kravtsov, A. V., Klypin, A. A., Porciani, C., & Primack, J. R., 2001, ApJ, 555, 240
Chen, H.-W., Lanzetta, K. M., Webb, J. K., & Barcons, X. 2001, ApJ, 559, 654
Chen, H.-W., & Tinker, J. L. 2008, ApJ, 687, 745
Collins, J. A., Shull, J. M., & Giroux, M. L. 2005, ApJ, 623, 196
Conroy, C., & Ostriker, J. P. 2008, ApJ, 681, 151
Croton, D. J. et al. 2006, 365, 11
Davé, R., Oppenheimer, B. D., & Sivanandam, S. 2008, MNRAS, 1190
Dekel, A. & Birnboim, Y. 2006, MNRAS, 368, 2
Dekel, A., & Birnboim, Y. 2008, MNRAS, 383, 119
Dekel, A., & Silk, J. 1986, ApJ, 303, 39
Dove, J. B., Shull, J. M., & Ferrara, A. 2000, ApJ, 531, 846
Fang, T., Mckee, C. F., Canizares, C. R., & Wolfire, M., 2006, ApJ, 644, 174
Ferland, G. J., Korista, K. T., Verner, D. A., Ferguson, J. W., Kingdon, J. B., & Verner, E. M., 1998, PASP, 110, 761
Field, G. B. 1965, ApJ, 142, 531
Fraternali, F., & Binney, J. J. 2008, MNRAS, 386, 935
Fukugita, M., & Peebles, P. J. E 2006, ApJ, 639, 590
Grcevich, J., Putman, M., & Peek, J. E. G. 2008, The Evolution of Galaxies Through the Neutral Hydrogen Window, 1035, 159
Kaufmann, T., Mayer, L., Wadsley , J., Stadel, J., Moore, B., 2006, MNRAS, 370, 1612
Kaufmann, T., Mayer, L., Wadsley, J., Stadel, J., & Moore, B. 2007, MNRAS, 375, 53
Kacprzak, G. G., Churchill, C. W., Steidel, C. C., & Murphy, M. T. 2008, AJ, 135, 922
Katz, N. 1992, ApJ, 391, 502
Katz, N., Weinberg, D. H., & Hernquist, L. 1996, ApJS, 105, 19
Kazantzidis, S., Magorrian, J., & Moore, B., 2004, ApJ, 601, 37
Kennicutt, R. C., Jr., 1998, ApJ, 498, 541
Kereš, D., Katz, N., Fardal, M., Davé, R., & Weinberg, D. H. 2009, MNRAS, 375
Kereš, D., Katz, N., Weinberg, D. H., & Davé, R. 2005, MNRAS, 363, 2
Khochfar, S., & Ostriker, J. P. 2008, ApJ, 680, 54
Li, Z., Wang, Q. D., & Hameed, S., 2007, MNRAS, 376, 960
Li, J.-T., Li, Z., Wang, Q. D., Irwin, J. A., & Rossa, J. 2008, MNRAS, 390, 59
Lu, Y., & Mo, H. J. 2007, MNRAS, 377, 617
Maller, A. H., & Dekel, A. 2002, MNRAS, 335, 487
Maller, A. H. & Bullock, J. S. 2004 MNRAS, 355, 694
Maller, A. H., Katz, N., Kereš, D., Davé, R., & Weinberg, D. H. 2006, ApJ, 647, 763
Maloney, P. 1993, ApJ, 414, 41
Maloney, P. R., & Putman, M. E. 2003, ApJ, 589, 270
Mastropietro, C., Moore, B., Mayer, L., Wadsley, J., & Stadel, J. 2005, MNRAS, 363, 509
Mo, H. J., & Miralda-Escude, J. 1996, ApJ, 469, 589
Mo, H. J., & Mao, S. 2002, MNRAS, 333, 768
Mo, H. J., Yang, X., van den Bosch, F. C., & Katz, N. 2005, MNRAS, 363, 1155
Monaghan, J. J. 1992, ARAA, 30, 543
Murphy, E. M., Lockman, F. J., & Savage, B. D. 1995, ApJ, 447, 642
Murray, S. D., White, S. D. M., Blondin, J. M., Lin, D. N. C., 1993, ApJ, 407, 588
Navarro, J. F., Frenk, C. S., & White, S. D. M., 1996, ApJ, 462, 563
Navarro, J. F., & Steinmetz, M. 2000, ApJ, 538, 477
Nicastro, F., Mathur, S., & Elvis, M. 2008, Science, 319, 55
Oh, S. P., & Benson, A. J. 2003, MNRAS, 342, 664
Oppenheimer, B. D. & Davé, R. 2006, MNRAS, 373, 1265
Pedersen, K., Rasmussen, J., Sommer-Larsen, J., Toft, S., Benson, A. J., & Bower, R. G., 2006, New Astronomy, 11, 465
Peek, J. E. G., Putman, M. E., McKee, C. F., Heiles, C., & Stanimirović, S. 2007, ApJ, 656, 907
Putman, M. E. 2006, ApJ, 645, 1164
Rand, R. J., & Benjamin, R. A. 2008, ApJ, 676, 991
Sancisi, R., Fraternali, F., Oosterloo, T., & van der Hulst, T. 2008, A&ARv, 15, 189
Sembach, K. R., et al. 2003, ApJS, 146, 165
Slavin, J. D., McKee, C. F., & Hollenbach, D. J. 2000, ApJ, 541, 218
Sommer-Larsen, J. 2006, ApJ, 644, L1
Stadel J., 2001, PhD Thesis, U. Washington
Steidel, C. C. 1995, QSO Absorption Lines, 139
Sternberg, A., McKee, C. F., & Wolfire, M. G., 2002, ApJS, 143, 419

Stewart, K. R., Bullock, J. S., Wechsler, R. H., Maller, A. H., & Zentner, A. R. 2008, ApJ, 683, 597
Tang, S., Wang, Q. D., Lu, Y., & Mo, H. J. 2009, MNRAS, 392, 77
Thom, C., Putman, M. E., Gibson, B. K., Christlieb, N., Flynn, C., Beers, T. C., Wilhelm, R., & Lee, Y. S. 2006, ApJ, 638, L97
Toft, S., Rasmussen, J., Sommer-Larsen, J., & Pedersen, K. 2002, MNRAS, 335, 799
Tripp, T. M., et al. 2003, AJ, 125, 3122
Tripp, T. M., & Bowen, D. V. 2005, IAU Colloq. 199: Probing Galaxies through Quasar Absorption Lines, 5
Tumlinson, J., & Fang, T. 2005, ApJ, 623, L97
van den Bosch, F. C. 2001, MNRAS, 327, 1334
Vieser, W., & Hensler, G. 2007, A&A, 472, 141
Vietri, M., Ferrara, A., & Miniati, F. 1997, ApJ, 483, 262
Wadsley J., Stadel J., Quinn T., 2004, NewA, 9, 137
Wang, Q. D., et al. 2005, ApJ, 635, 386
Wechsler, R. H., Bullock, J. S., Primack, J. R., Kravtsov, A. V., & Dekel, A. 2002, ApJ, 568, 52
White, S. D. M., & Rees, M. J. 1978, MNRAS, 183, 341
Williams, R. J., et al. 2005, ApJ, 631, 856
Zemp, M., Moore, B., Stadel, J., Carollo, C. M., & Madau, P. 2008, MNRAS, 386, 1543
Zhao, D. H., Jing, Y. P., Mo, H. J., & Boerner, G. 2008, arXiv:0811.0828